

Investigation of Path-Dependent Degradation in Lithium-Ion Batteries**

Trishna Raj,^[a] Andrew A. Wang,^[a, b] Charles W. Monroe,^[a, b] and David A. Howey^{*,[a, b]}

Models that predict battery lifetime require knowledge of the causes of degradation and operating conditions that accelerate it. Batteries experience two ageing modes: calendar ageing at rest and cyclic ageing during the passage of current. Existing empirical ageing models treat these as independent, but degradation may be sensitive to their order and periodicity – a phenomenon that has been called “path dependence”. This experimental study of path dependence probes whether interactions between ageing conditions can impact a battery’s

state of health. Groups of graphite/NCA 18650 lithium-ion cells were exposed to load profiles consisting of similar proportions of calendar and cyclic ageing applied in various orders. Load profiles at higher C-rates exhibited path dependence, which differential voltage analysis correlates with increased anode degradation. These results suggest that more accurate ageing models should include the possible coupling between calendar and cyclic ageing modes.

1. Introduction

Advances in battery technology are making electric vehicles (EVs) an attractive and viable transport option. Energy storage technology has improved greatly in recent years, with lithium-ion (Li-ion) batteries achieving higher energy density, higher power density, higher cell voltage and lower self-discharge rate than the previous nickel metal hydride technology.^[1] An ideal EV battery should not only offer high performance but should also be durable, with minimal capacity and power fade during its useful life.^[2,3] The energy density of batteries is constantly improving: the latest EVs have batteries with a pack energy density of 150 Wh/kg, compared to less than 100 Wh/kg a decade ago.^[4] Lifetime prediction continues to be challenging, especially for cells operating under real driving conditions, where lifetime is affected by factors such as external temperature, pack cooling, intensity of usage, etc.^[5] Understanding how different conditions impact cell ageing can enable new methods of lifetime and performance prediction. Accurate prediction benefits both consumers and manufacturers, and is essential for long-term applications such as EVs and grid energy storage systems.

Empirically, batteries can be described as experiencing “calendar ageing” (at open circuit) and “cyclic ageing” (at non-zero applied current). In the case of an EV, calendar ageing occurs when the vehicle is parked, while cyclic ageing occurs during driving and charging. The influence of each of these conditions on cell degradation has been studied by considering calendar and cyclic ageing to be independent.^[6–9] Empirical ageing models either account for only a single mode of ageing (calendar or cyclic)^[10,11] or treat these modes separately and add their contributions together to form a combined model.^[12–14]

It has been suggested by Dubarry et al.^[15] that there may be a so-called “path dependence” effect, which is to say, separately considering and then summing the impacts of calendar and cyclic ageing may not be valid, leading to inaccurate lifetime predictions. It is possible to investigate this hypothesis by testing batteries under combined loading profiles. Ma et al.^[16] identified that the accuracy of state-of-health estimation might be impacted by path dependence, and explored this experimentally. Six pairs of cells were aged using a drive cycle under various thermal conditions and cycling to various depths of discharge. Since the cells were exposed to three different stress factors, however, it is unclear whether their degradation was caused by the environmental temperature, the discharge-depth variations, or by cell heating due to dynamic cycling. Dubarry et al.^[15,17] created an experimental campaign incorporating cycling related to EV driving, EV recharging, calendar ageing during parking, and vehicle-to-grid/grid-to-vehicle usage. To accelerate ageing, the profiles were simplified, which resulted in calendar ageing periods being shorter compared to a real-world scenario. Due to the accelerated conditions used, the influence of path dependence is unclear. Finally, a study of path dependence was attempted by Gering et al.,^[18] including an investigation of how power pulses influence degradation. Five groups of cells were exposed to charge/discharge power pulses that varied in amplitude and duration. The tests incorporated calendar-ageing periods of varying duration, and

[a] T. Raj, A. A. Wang, Prof. C. W. Monroe, Prof. D. A. Howey
Department of Engineering Science
University of Oxford

[b] A. A. Wang, Prof. C. W. Monroe, Prof. D. A. Howey
The Faraday Institution
Becquerel Avenue, Harwell Campus,
Didcot, OX11 0RA, United Kingdom
E-mail: david.howey@eng.ox.ac.uk

[**] Data sets presented in this paper are available at Oxford Research Archive, <https://doi.org/10.5287/bodleian:v0ervBv6p> (DOI: 10.5287/bodleian:v0ervBv6p).

© 2020 The Authors. Published by Wiley-VCH GmbH. This is an open access article under the terms of the Creative Commons Attribution License, which permits use, distribution and reproduction in any medium, provided the original work is properly cited.

the comparability of results was ensured by keeping the cumulative discharge energy consistent across tests, but conclusive long-term results were not given.

This paper presents a long-term ageing study to elucidate the path dependence of commercially available lithium-ion 18650 cells with nickel cobalt aluminium oxide (NCA) positive electrodes and graphite negative electrodes. Groups of cells were subjected to load profiles comprising fixed periods of calendar and cyclic ageing applied in various orders. Incremental capacity analysis (ICA) and differential voltage analysis (DVA) were used to evaluate differences in the resulting degradation. Results indicate that path dependence does exist, particularly when cells are exposed to current-controlled cycling at higher rates. In this case, differences between groups of cells were observed in DVA peaks at lower voltages, corresponding with negative electrode DVA features. These are shown to be related to loss of active material in the negative electrode.

2. Experimental Section

The experimental campaign used here was designed to combine calendar and cyclic ageing periods while minimizing the influences of other stress factors, notably temperature extremes. To ensure that the observed effects were relevant to practical applications in EVs, tests were conducted at temperatures reflective of a well-managed battery system.

2.1. Cells and Equipment

Panasonic NCA/graphite 18650 lithium-ion cells were used for experiments; Table 1 details the cell specification. To give an indication of cell-to-cell variability but not use a prohibitive number of test channels, three cells were tested at each of the 4 experimental conditions, for a total of 12 cells required.

A battery tester (Maccor 4200) was used to cycle the cells and to conduct the reference performance tests (RPTs). Additionally, electrochemical impedance spectroscopy (EIS) tests at the beginning of life (BoL), middle of life (after 384 days), and end of life were conducted using a potentiostat (BioLogic MPG205). To ensure accurate voltage measurement, cells were tested in 4-terminal holders with separate power and sense pins. Throughout characterization and testing, cells were kept at a constant ambient temperature of 24 °C inside a thermal chamber (Binder MK 53).

Table 1. Specifications of the Li-ion cells used in the experimental campaign.	
Parameter	Value
Manufacturer Code	NCR18650BD
Cathode	LiNiCoAlO ₂ (NCA)
Anode	Carbon
Rated Capacity	3 Ah
Maximum Voltage	4.2 V
Minimum Voltage	2.5 V
Maximum Charge Current	1.5 A
Maximum Continuous Discharge Current	10 A

2.2. Degradation Ageing Profiles

All four groups were subjected to a 1:5 ratio of cyclic to calendar ageing periods, but these periods were staged in different orders and cycling was performed at different C-rates. (In this work, C-rate is always based on rated capacity, rather than actual capacity, and follows the usual definition, namely current divided by capacity). The combined load-profile conditions are presented schematically in Figure 1(a). Cells in groups 1 and 2 were periodically exposed to one day of cycling followed by five days of calendar ageing. Cells in groups 3 and 4 were periodically exposed to two days of cycling followed by ten days of calendar ageing. To probe whether C-rate influences path dependence, the cycling for groups 1 and 3 was conducted at a C-rate of C/2 while groups 2 and 4 were cycled at C/4.

Cells in all four groups were cycled between 0% and 100% state of charge (SoC), i.e. 2.5–4.2 V. Cycling was conducted by applying a constant current during charge and discharge steps. This was selected instead of a dynamic drive cycle to expose the cells to the simplest possible continuous cycling profile, with equal time spent at all SoCs. Since dynamic drive cycles are usually realistic representations of EV driving, they tend to incorporate factors such as regenerative braking, which produce high-power spikes that can introduce unexpected stress factors specific to the drive cycle chosen. Calendar ageing was always performed at 90% of actual SoC. As cycling periods ran, the SoC for each cycle was re-normalised by the capacity achieved in the prior cycle. More concretely, the number of amp-hours passed between 2.5–4.2 V was saved as a variable that was updated after each charge or discharge step. This variable was used to determine the length of time needed to discharge 10% of the prior-cycle capacity. A relatively high SoC was selected for calendar ageing to promote degradation.

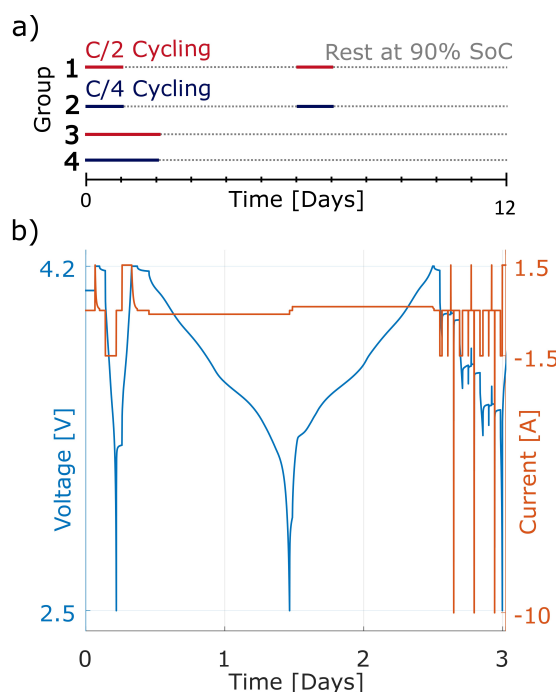


Figure 1. a) Load profiles, with groups 1 and 3 cycled at C/2 and groups 2 and 4 cycled at C/4, with calendar ageing conducted at 90% SoC. b) RPT current profile and cell voltage response conducted every 48 cycles.

2.3. Reference Performance Tests

Reference performance tests were conducted every 48 cycles to quantify changes in capacity and internal resistance associated with degradation. These tests were synchronized with respect to cycles instead of calendar time, ensuring that the cells experienced the same charge throughput across all groups between RPTs. (This means that groups 2 and 4 experienced half the number of RPTs in time compared to groups 1 and 3.)

The RPT procedure is shown in Figure 1(b). Each test started with a 3-hour open-circuit relaxation to allow thermal equilibration. The capacity under load was estimated using a constant current-constant voltage (CCCV) test at C/2 until the current was C/60 (0.05 A). Then a pseudo-open-circuit-voltage (pseudo-OCV) test was conducted at C/24. Here, pseudo-OCV is defined to mean data measured during a low rate cycle, as is common in the literature.^[19] Pseudo-OCV measurements are not the same as true OCV measurements, since the latter require the cell to be relaxed and at zero current. Nonetheless, pseudo-OCV measured by low rate cycling minimises internal overpotentials and is sufficiently close to true OCV that it gives an accurate representation of cell capacity and can be used for DVA and ICA. The pseudo-OCV measurement was followed by a pulse-power characterization (PPC) test to study the voltage response of the cell when exposed to current pulses, and to estimate the DC ohmic resistance. The PPC was conducted at 80%, 50% and 20% SoC with 10-second pulses of C/2 (1.5 A) charge and discharge, and 3.33 C (10 A) discharge at each SoC. (The SOC change during the 10 A power pulse was taken into consideration when resetting to the next SOC point.) The DC resistance was calculated with Equation (1):

$$R_{DC} = \frac{V_{10s} - V_{0s}}{I_{pulse}} \quad (1)$$

in which R_{DC} is the DC resistance, I_{pulse} is the pulse current, and V_x is the voltage at time x after the start of the pulse.

Additionally, cells were characterized at BoL and end-of-life through more extensive tests, including the galvanostatic intermittent titration technique (GITT) as well as EIS. GITT was conducted at C/2 in 10% SoC intervals (based on actual capacity) from the fully charged (4.2 V) to the fully discharged (2.5 V) condition. EIS was conducted with a 100 mA peak-to-peak excitation amplitude in the frequency range of 5 kHz to 10 mHz, with a resolution of 6 points per decade. EIS was performed at 80%, 50% and 20% SoC, based on the most recent RPT capacity.

2.4. Half Cells

To gain insight into the influence of each electrode on degradation, half cells were assembled using electrode material harvested from a fresh 18650 cell. Electrodes of area 4.52 cm² were cleaned and punched (MSK-T-10 Precision Disc Cutter) from the 726 cm² of extracted electrode material. Method 2, as described by Schmid et al.,^[20] was followed to clean the electrode material and construct the half cells. CR2032 half-cells were constructed with lithium foil as the counter electrode, the punched electrode material, LP30 electrolyte consisting of 1.0 M LiPF₆ solution in 50/50 ethylene carbonate and dimethyl carbonate, and Celgard 2400 separator material. Pseudo-OCV measurements were conducted on the half-cells at C/24 at room temperature. The cathode half-cell was tested between 2.49 V vs. Li+/0 and 4.29 V vs. Li+/0, and the pseudo-OCV test on the anode was conducted between 0.04 V vs. Li+/0 and 1.25 V vs. Li+/0.

3. Results

Path dependence can be studied by comparing results from groups 1 and 3, or groups 2 and 4, since these pairs experienced the same amounts of calendar and cyclic ageing, but in different orders. As a reminder, group 1 experienced 1 day of cycling at C/2 followed by 5 days of calendar ageing, while group 3 experienced 2 days of cyclic ageing at C/2 followed by 10 days of calendar ageing. Similarly, group 2 experienced 1 day of cycling at C/4 followed by 5 days of calendar ageing, and group 4 experienced 2 days of cycling at C/4 followed by 10 days of calendar ageing.

The normalized RPT data from all four groups of cells is shown in Figure 2(a)–(b), plotted separately against time and full equivalent cycles (FEC). Capacity was normalized by the measured capacity at BoL, i.e., as Q_{actual}/Q_{BoL} . There is a divergence in ageing behaviour between groups 1 and 3, with the latter experiencing a higher rate of capacity fade. Group 3 incurs an average of 17% capacity loss by the end of the experiment, while group 1 loses 13% on average. The rate of capacity fade for groups 2 and 4 is similar, however, with both groups experiencing an average of 10% capacity loss over the experimental period. The similar capacity fade observed between groups 2 and 4 may suggest that path dependence is less important at lower C-rates. Figure 2(c)–(d) presents the instantaneous DC resistance R_{actual} , expressed as a fractional change relative to the DC resistance measured at BoL, i.e., as $(R_{actual} - R_{BoL})/R_{BoL}$. The resistance data correlates with the trends seen in the capacity data. Group 3 experiences a higher rate of resistance increase than group 1, whereas groups 2 and 4 show similar rates of increase. To gain further insight into the change in resistance as the cells age, the BoL and middle of life (MoL) EIS data at 50% SoC are given in Figure 3, which shows the impedances in groups 1 and 3 increasing at different rates. This supports the resistance data in Figure 2, showing the influence of path dependence on power fade.

The degradation trajectories within each group diverge from one another due to cell-to-cell variability, which studies have shown can be significant.^[21] This is likely caused by manufacturing inconsistencies, and this spread is larger for groups 1 and 3 which were cycled at higher C-rates.

4. Analysis and Discussion

Figure 2 shows data confirming that at higher C-rates, path dependence influences the amounts of both capacity fade and resistance increase. There is little or no difference in the degradation trajectories of cells tested at C/4 (groups 2 and 4), but a discernible difference in those of cells tested at C/2 (groups 1 and 3). Generally, the percentage resistance increase is far higher than the percentage of capacity lost, rising faster with both time and cycling.

Cells in group 3 experienced continuous cycling for a longer amount of time, which could incur a greater build-up of mechanical consequences within the electrodes, such as particle cracking and loss of electrical contact. These phenom-

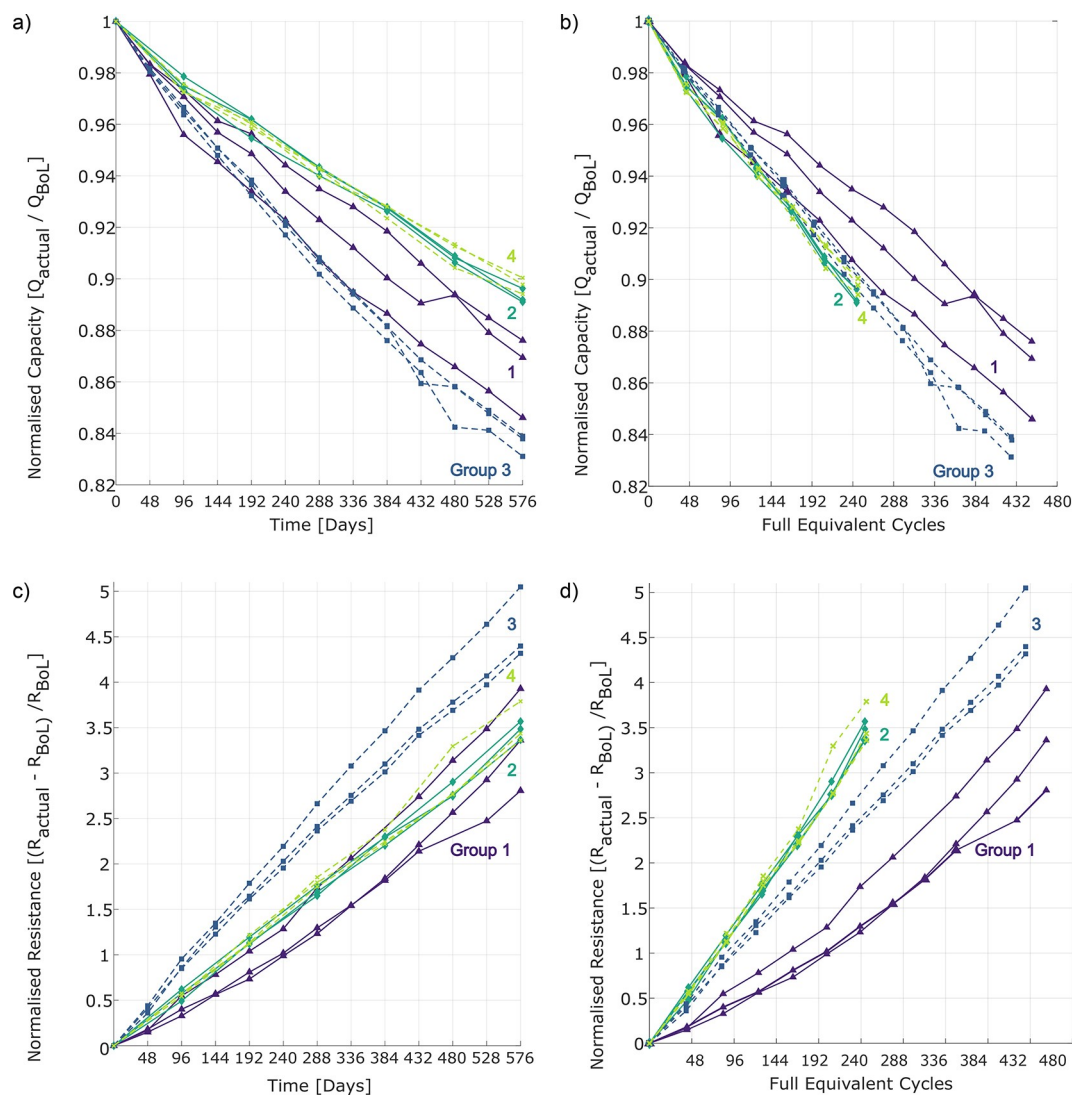


Figure 2. Discharge capacity (measured by pseudo-OCV) for all test groups schematized in Figure 1(a), vs. a) time and b) full equivalent cycles; resistance data (measured by PPC) for the same groups, against c) time and d) full equivalent cycles.

ena both incur capacity fade by loss of active material. Studies of the influence of cycling on volume expansion of electrode materials show that during a charge or discharge graphite experiences a 10% volume change, while the NCA electrode volume changes by 4.5%.^[22] Mechanical degradation caused by longer continuous cycling in group 3 would therefore be expected to have a greater effect on the anode.

Groups 2 and 4, cycled at C/4, experienced a lower rate of fade with respect to time compared to groups 1 and 3 respectively, cycled at C/2. This was expected, since these cells only experienced half the number of full equivalent cycles that the cells in groups 1 and 3 did. In contrast, when viewed as a function of full equivalent cycles (charge throughput), groups 2 and 4 show a higher rate of capacity fade than groups 1 and 3, respectively. This could be because groups 2 and 4, which cycled slower, spent a longer time at voltage extremes than groups 1 and 3 – an electrochemical stressor known to accelerate degradation.^[23,24] Trends in the resistance data are similar, with groups 2 and 4 experiencing a lower rate of

degradation with respect to time, but a higher rate of degradation versus full equivalent cycles.

ICA and DVA analyses were conducted using the pseudo-OCV data collected from the RPTs to clarify the degradation mechanism associated with path dependence. ICA uses plots of dQ/dV versus V to elucidate electrode-specific thermodynamic changes, whereas DVA uses plots of dV/dQ versus Q to evaluate loss of active material and cyclable lithium. More specifically, the staged intercalation of lithium in the graphite negative electrode, and the phase transitions associated with lithiation of the metal-oxide positive electrode manifest as features (peaks or valleys) in the ICA and DVA plots.^[16,25] Observation of the shifting and shrinking of particular features as the cell ages enables the quantification of lost lithium inventory, and also provides separate estimates of the loss of active material in the positive electrode and negative electrode.^[26–28]

Figure 4 shows the ICA signatures of representative cells from all four groups, with the features of interest denoted P1–P4. The cell that experienced the least degradation in each

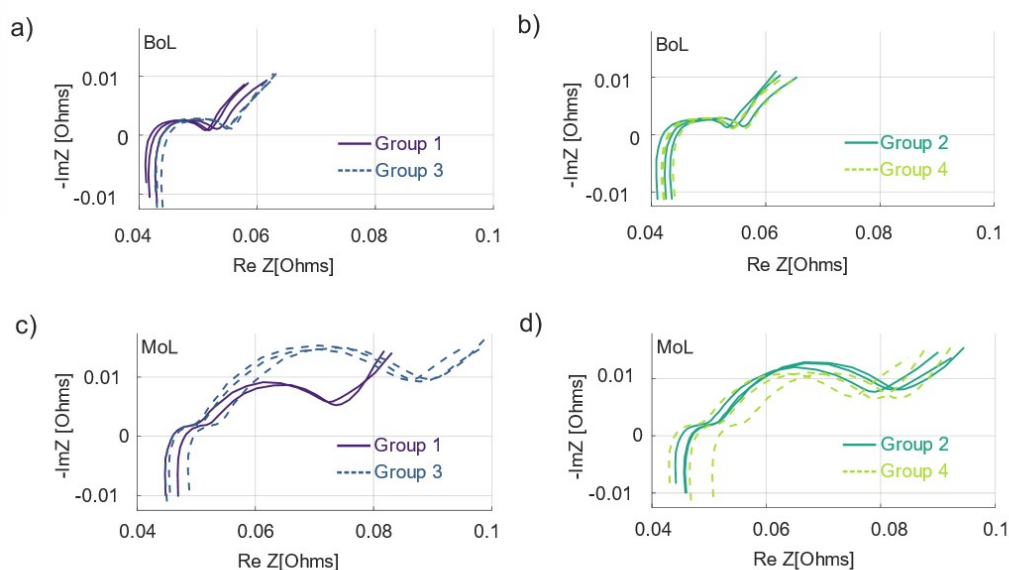


Figure 3. Beginning-of-life impedance spectra for a) groups 1 & 3 and b) groups 2 & 4; middle-of-life spectra for c) groups 1 & 3 and d) groups 2 & 4.

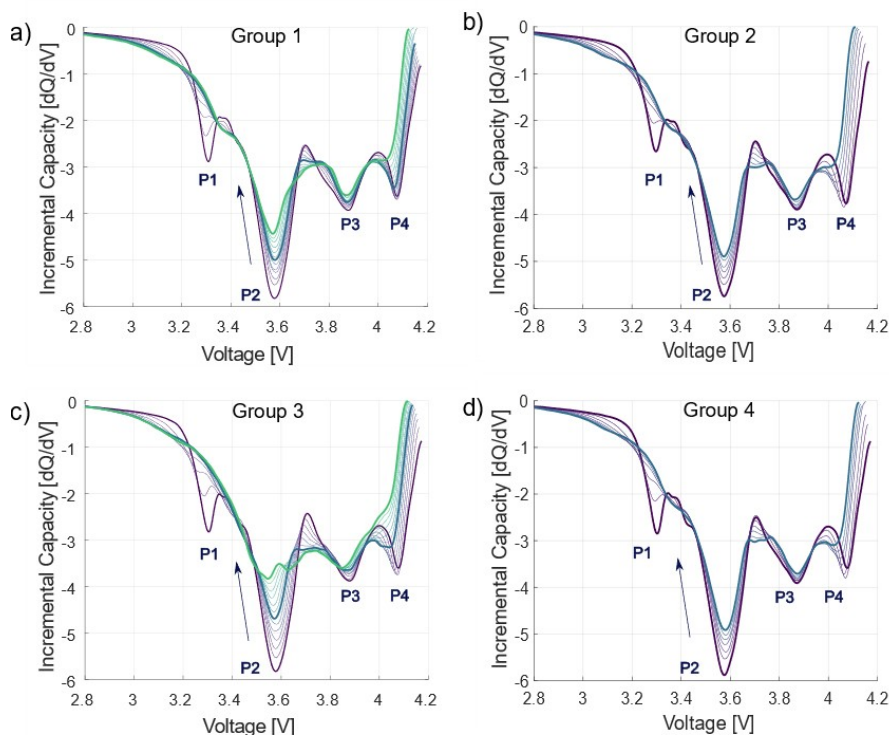


Figure 4. Progression of ICA during ageing for a) group 1, b) group 2, c) group 3 and d) group 4 (arrow direction indicates ageing), thick blue line is 7th RPT.

group was selected as the representative cell for ICA/DVA. This ensures that the comparison between groups is not artificially exaggerated. The BoL ICA plots (purple lines) for all groups show similar feature heights and positions. As the cells in

groups 1 and 3 age, the features diminish in height and shift towards lower voltages at different rates. Group 3 experiences a higher rate of change in feature heights compared to group 1, and this difference may be attributed to path dependence.

The changes in the peak height and shift of the features of interest in groups 2 and 4 are similar to one another, supporting the similar overall degradation trends seen in Figure 2. Figure 5 shows the difference between the initial ICA signatures for groups 1 and 3 and the difference between the final signatures. There is little difference at the beginning of life, but as the cells age, a significant difference between groups emerges, particularly in features P1, P2 and P4. The shrinking of features P1 and P2 can be related to loss of electrode active material,^[29] while the shift and shrink of P4 can be attributed to loss of lithium inventory.^[22] However, it is not possible from the ICA signatures to determine which specific electrode is losing active material.

To further clarify this, half-cell data and DVA were used to attribute changes to the anode or the cathode.^[11,30] DVA was conducted using the pseudo-OCV data from the pristine half-cells described in section 2. Half-cell data was normalized by the active electrode area in the coin cells, to produce a SoC that could be meaningfully compared to the SoC of the 18650 cells.

The results presented in Figure 6 indicate that features P1 and P2 of a full-cell DVA signature collected from a pristine cell

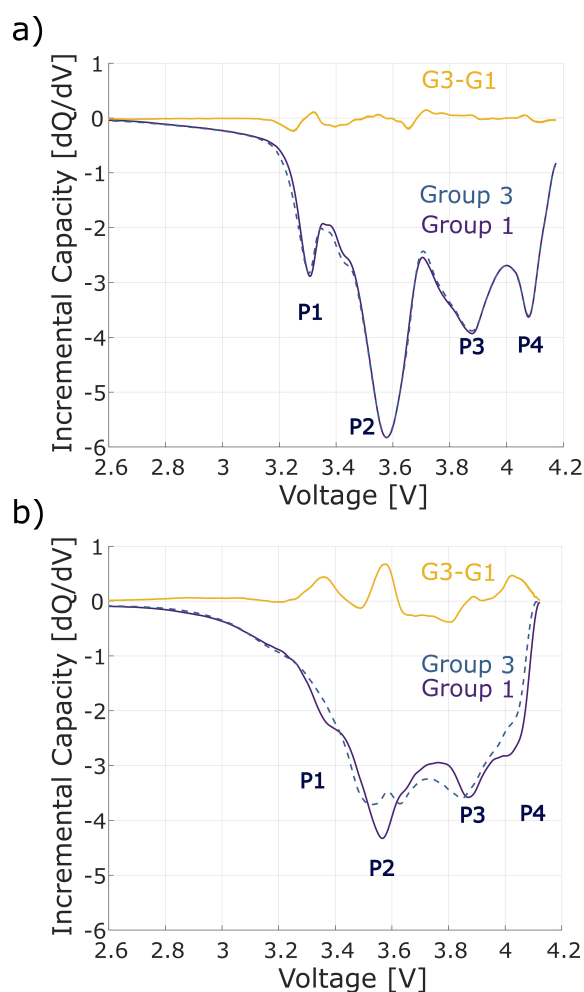


Figure 5. Difference between ICA signatures of Groups 1 and 3 a) at the beginning of life and b) at the most recent RPT.

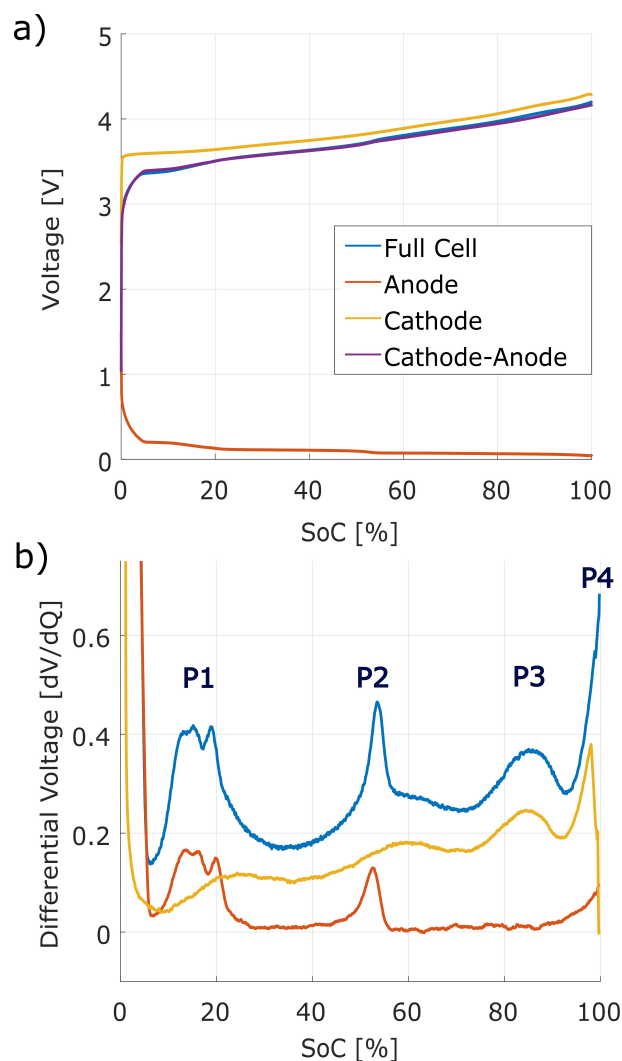


Figure 6. a) Pseudo-OCV curves for a pristine full cell, half cells constructed from pristine cell material, and the difference between the half-cell pseudo-OCV curves. b) DVA signatures of the same.

can be attributed to the anode, while the cathode governs the higher SoC voltages attributed to P3 and P4. Reduction in the heights of the P1 and P2 features is therefore attributable to loss of negative electrode material. Thus the loss of active material at the negative electrode likely plays a more prominent role in path-dependent degradation under the conditions tested in this work. Loss of active negative electrode material could be a result of microcracks forming. Loss of lithium inventory results in the shift of P4 in the ICA signature. This could result from growth of the solid electrolyte interphase, but may also be due to loss of lithiated electrode material. Comparing the ICA and the DVA signatures (Figure 7) with those simulated for a cell of the same chemistry by Dubarry et al.^[22] confirms that the difference in the rate of degradation between groups 1 and 3 could be due to differing rates of loss of lithiated negative electrode active material.

Full-cell DVA signatures for all four groups, presented in Figure 7, can be used to quantify the capacity loss attributed to each electrode, while also giving insight into the cell's

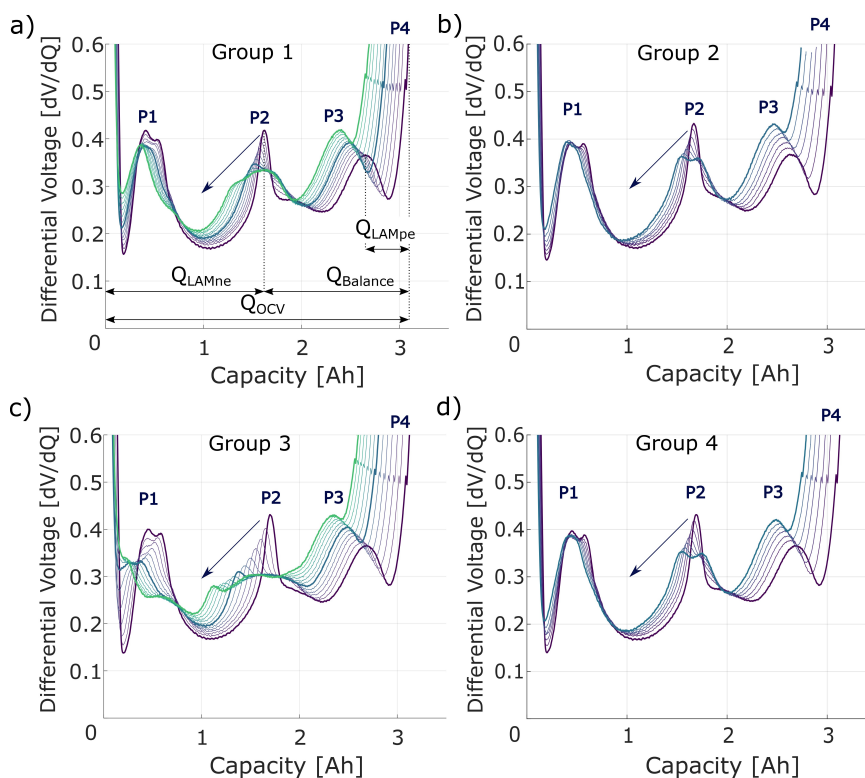


Figure 7. Progression of DVA signatures as the cell ages for a) Group 1 with characteristic capacities annotated below the signatures and b) Group 2, c) Group 3 and d) Group 4 (arrow direction indicates ageing).

electrode balancing.^[31] Keil et al.^[31] suggest there are characteristic capacities that can be estimated to determine the change in electrode balancing and the loss of active material at the negative and positive electrodes (LAMne and LAMpe respectively). The former can be identified as the change in capacity between 0% SoC and P2, indicated in Figure 7 as Q_{LAMne} , since all the features of interest in this range are anode specific. Similarly, the latter, Q_{LAMpe} can be determined by the change in capacity between P3 and 100% SoC. Changes in the electrode balancing (Q_{Balance}) and the impact of loss of lithium inventory can be identified by calculating the capacity changes between P2 and 100% SoC.

The DVA signatures confirm that cells cycled at C/4 (groups 2 and 4) experienced the same degradation modes, at similar rates to each other, whereas cells cycled at C/2 (groups 1 and 3) show very different trajectories to each other. The thicker blue line in all sub-figures corresponds to the 7th RPT, at approximately 240 FEC. This facilitates comparison between groups as a function of FEC. However, since groups 2 and 4 experienced half the number of RPTs in time compared to groups 1 and 3, time-based comparisons should be made using the *final* DVA signatures in all cases. Comparing the cells cycled at different rates (groups 1 vs. 2; 3 vs. 4) versus time, cells cycled at C/2 experienced a greater loss of negative electrode active material, seen in P1 and P2, compared to cells cycled at C/4. The difference in the loss of negative electrode active material is pronounced when comparing the cells cycled for a longer continuous duration under different rates (i.e., group 3

vs. 4). With respect to time, the cells cycled at a higher rate also experienced a greater change in Q_{Balance} indicating a difference in the loss of lithium inventory. However, as a function of FEC, a comparison between groups 1 and 2 shows differences particularly around P3 and P4, perhaps indicating that at lower rates calendar ageing effects caused by time spent at high voltage may be important, as was previously noted. On the other hand, a comparison between groups 3 and 4 as a function of FEC indicates more of a difference at P1 and P2, showing that the increased C-rate has led to a completely different degradation mode, likely associated with negative electrode material lost as already discussed.

Figure 8 summarises the characteristic capacities from each DVA at each RPT for groups 1 and 3, and shows that the anode (Q_{LAMne}) experiences the most significant difference in electrode degradation. This can be attributed to a loss of active material that accompanies the expected loss of lithium inventory, leading to an imbalance of the electrodes.

5. Conclusions

To investigate degradation path dependence and its influence on state of health, an experimental study was conducted using combined calendar and cyclic ageing profiles designed to isolate this issue. Four groups of cells were subjected to the same ratio of calendar to cyclic ageing, but the ordering of the

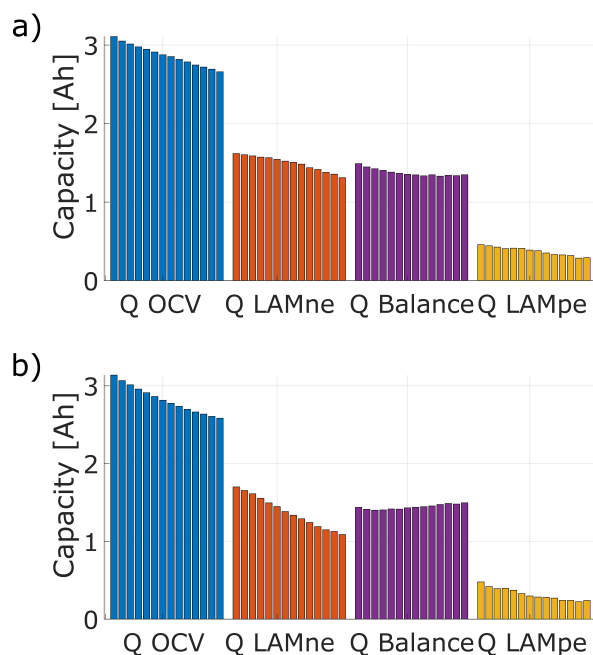


Figure 8. DVA peak analysis for a) Group 1 and b) Group 3 (progression in time shown left to right within each sub-metric).

two ageing modes and the C-rate of the cycling was varied between groups.

Capacity data collected during reference performance tests with the pseudo-OCV technique revealed a significant divergence in the degradation paths between groups 1 and 3 (at C/2), whereas groups 2 and 4 (at C/4) showed very little difference in their degradation rates. This indicates that path dependence is rate dependent, with no influence exhibited at lower C-rates, but a difference in degradation trajectories seen at higher C-rates. Resistance data supported the interpretation of the capacity-fade data, displaying identical trends. When expressed as a fractional change relative to initial values, path dependence appeared to influence the increase of resistance more strongly than the decrease in capacity.

The ICA and DVA data comparing groups 2 and 4 confirmed that the cells cycled at the lower rate degraded with similar degradation mechanisms. The IC/DV analysis conducted on groups 1 and 3 however showed that the features of interest change at different rates, with group 3 experiencing a faster rate of feature shift and shrink rate. The impact of ageing on the individual electrodes was studied by comparing DVA of the aged cells to similar data gathered from half cells. The difference in ICA signatures between groups of cells aged at C/2 suggests that path-dependent degradation results in the loss of lithium inventory and the loss of active material in the lower-to-middle voltage range, which half-cell DVA indicates is dominated by the anode. This was further confirmed with full cell DVA, which also showed that the greatest difference occurs at the negative electrode. From the analysis, the difference in degradation specifically related to path dependence could be

attributed to an increased loss of lithiated active material at the negative electrode, perhaps due to electrode cracking and loss of electrical contact.

We conclude that higher C-rates and longer durations of continuous cycling without rest periods could accelerate degradation when measured with respect to time, beyond what might be expected based on models that take the effects of calendar and cyclic ageing to be both cumulative and independent. The sequencing of ageing tests may influence the rate of degradation, especially at high C-rates. The assumption that calendar and cyclic ageing test data can simply be superimposed in empirical ageing studies may be inaccurate at higher C-rates and during continuous cycling. By incorporating this understanding of path dependence into lifetime degradation models, the accuracy of lifetime predictions for Li-ion batteries in EVs could be improved.

Acknowledgements

The authors gratefully acknowledge the financial support of EPSRC UK, The Faraday Institution, and Jaguar Land Rover, and thank Dr. Jorge Varela Barreras with early assistance in setting up the tests.

Conflict of Interest

The authors declare no conflict of interest.

Keywords: degradation · ageing · lithium-ion · battery · energy conversion · electrochemistry

- [1] A. Ritchie, W. Howard, *J. Power Sources* **2006**, *162*, 809–812.
- [2] A. Affanni, A. Bellini, G. Franceschini, *IEEE T. Ind. Electron.* **2005**, *52*, 1343–1349.
- [3] "Lithium-ion Batteries for Electric Vehicles: the U.S. Value Chain", *Duke University Center on Globalization, Governance & Competitiveness*, M. Lowe, S. Tokunaka, T. Trigg, G. Gereffi **2010**, 1–76.
- [4] B. Nykvist, F. Sprei, M. Nilsson, *Energ. Policy* **2018**, *124*, 144–155.
- [5] F. Yang, Y. Xie, Y. Deng, C. Yuan, *Nat. Commun.* **2018**, *9*, 1–10.
- [6] J. C. Burns, A. Kassam, N. N. Sinha, L. E. Downie, *J. Electrochem. Soc.* **2013**, *160*, A1451–A1456.
- [7] S. Käbitz, J. B. Gerschler, M. Ecker, *J. Power Sources* **2013**, *239*, 572–583.
- [8] M. Kassem, J. Bernard, R. Revel, S. Pélissier, F. Duclaud, C. Delacourt, *J. Power Sources* **2012**, *208*, 296–305.
- [9] I. Bloom, B. W. Cole, J. J. Sohn, S. A. Jones, *J. Power Sources* **2001**, *101*, 238–247.
- [10] M. Ecker, J. B. Gerschler, J. Vogel, *J. Power Sources* **2012**, *215*, 248–257.
- [11] J. Wang, J. Purewal, P. Liu, *J. Power Sources* **2014**, *272*, 1154–1161.
- [12] E. Sarasketa-Zabala, E. Martinez-Laserna, M. Berecibar, I. Gandiaga, *Appl. Energy* **2016**, *162*, 839–852.
- [13] M. Schimpe, M. E. von Kuepach, M. Naumann, *ECS Trans.* **2017**, *80*, 147–170.
- [14] C. Guenther, B. Schott, W. Hennings, P. Waldowski, M. A. Danzer, *J. Power Sources* **2013**, *239*, 604–610.
- [15] M. Dubarry, G. Baure, A. Devie, *J. Electrochem. Soc.* **2018**, *165*, A773–A783.
- [16] Z. Ma, J. Jiang, W. Shi, W. Zhang, C. C. Mi, *J. Power Sources* **2014**, *274*, 29–40.
- [17] M. Dubarry, A. Devie, K. McKenzie, *J. Power Sources* **2017**, *358*, 39–49.
- [18] K. L. Gering, S. V. Sazhin, D. K. Jamison, *J. Power Sources* **2011**, *196*, 395–3403.

- [19] A. Barai, K. Uddin, M. Dubarry, L. Somerville, *Prog. Energy Combust. Sci.* **2019**, *72*, 1–31.
- [20] A. U. Schmid, M. Kurka, K. P. Birke, *J. Energy Storage* **2019**, *24*, 100732.
- [21] T. Baumhöfer, M. Brühl, S. Rothgang, D. U. Sauer, *J. Power Sources* **2014**, *247*, 332–338.
- [22] A. J. Louli, J. Li, S. Trussler, C. R. Fell, J. R. Dahn, *J. Electrochem. Soc.* **2017**, *164*, A2689–A2696.
- [23] K. J. Park, J. Hwang, H. Ryu, F. Maglia, *ACS Energy Lett.* **2019**, *4*, 1394–1400.
- [24] G. Ning, B. Haran, B. N. Popov, *J. Power Sources* **2003**, *117*, 160–169.
- [25] M. Dubarry, C. Truchot, B. Y. Liaw, *J. Power Sources* **2012**, *219*, 204–216.
- [26] C. R. Birkel, M. R. Roberts, E. McTurk, P. G. Bruce, D. A. Howey, *J. Power Sources* **2017**, *341*, 373–386.
- [27] M. Dubarry, M. Bercibar, A. Devie, D. Anseán, N. Omar, I. Villarreal, *J. Power Sources* **2017**, *360*, 59–69.
- [28] X. Han, M. Ouyang, L. Lu, J. Li, Y. Zheng, Z. Li, *J. Power Sources* **2014**, *251*, 38–54.
- [29] “Modern Battery Engineering: a Comprehensive Introduction”, *World Scientific Publishing*, K. P. Birke, S. Hahn, K. P. Birke, **2019**, 141–166.
- [30] I. Bloom, A. N. Jansen, D. P. Abraham, J. Knuth, *J. Power Sources* **2005**, *139*, 295–303.
- [31] P. Keil, A. Jossen, *J. Electrochem. Soc.* **2017**, *164*, A6066–A6074.

Manuscript received: July 6, 2020
Revised manuscript received: July 30, 2020
Accepted manuscript online: August 25, 2020
Version of record online: September 17, 2020